

# DIFFRACTIVE PHENOMENA

GIUSEPPE IACOBUCCI

*INFN sezione di Bologna, Via Irnerio 46, I-40126 Bologna, Italy*

*E-mail: giuseppe.iacobucci@desy.de*

The most recent theoretical and experimental results in the field of diffractive scattering are reviewed. A parallel between the two current theoretical approaches to diffraction, the DIS picture in the Breit frame and the dipole picture in the target frame, is given, accompanied by a description of the models to which the data are compared. A recent calculation of the rescattering corrections, which hints at the universality of the diffractive parton distribution functions, is presented. The concept of generalized parton distributions is discussed together with the first measurement of the processes which might give access to them. Particular emphasis is given to the HERA data, to motivate why hard diffraction in deep inelastic scattering is viewed as an unrivalled instrument to shed light on the still obscure aspects of hadronic interactions.

## 1 Introduction

Hadronic diffractive scattering was one of the most popular fields of study in high-energy physics thirty years ago. The reason is probably that Regge theory, at that time the leading theory of hadronic interactions, was able to describe diffractive processes in even more detail than more inclusive processes, such as the total cross section  $\sigma_{tot}$ . The advent of quantum chromodynamics (QCD), the quantum field theory of strong interactions, marked a new epoch, since the perturbative QCD (pQCD) treatment reaped a harvest of calculations and predictions in hadronic hard scattering that raised the strong interactions to a level of understanding comparable to that reached by the other interactions that form the Standard Model of particle physics. However, in high-energy scattering processes QCD is applicable only when perturbative methods can be used, i.e. in the presence of a *hard scale*. This situation corresponds to small distance processes, or, equivalently, large momenta involved ( $p_T^2, Q^2, \dots$ ). As a consequence, we are unable to use QCD to compute the bulk of hadronic interactions, i.e. the *soft* –or large distance– total, elastic and diffractive cross sections. What happens is that at large distances the QCD coupling  $\alpha_s$  becomes

large and the phenomenon of *confinement* of hadrons changes radically the colour radiation pattern, making the calculations unaccessible.

Traditionally, confinement is studied by the investigation of the binding forces between quarks, described in terms of interquark potentials, which allow to calculate *static* properties of hadrons, such as the masses. In high-energy hadronic scattering, there is a special class of events, that we call *hard diffraction*, in which a hard scale is present and, at the same time, an initial state hadron may emerge intact in the final state. For these events, the strong confinement forces prevail over the strong forces which tend to break up the hadrons. By studying this class of events, we hope to learn about the fundamental properties of the binding forces within hadrons.

In the following, mostly HERA data will be discussed, since the recent Tevatron data were already presented<sup>1</sup> at the Lepton-Photon conference two years ago. In the coming Tevatron Run II, both the D0 and CDF detectors will be instrumented with forward proton spectrometers, which will enhance their sensitivity to diffractive processes.

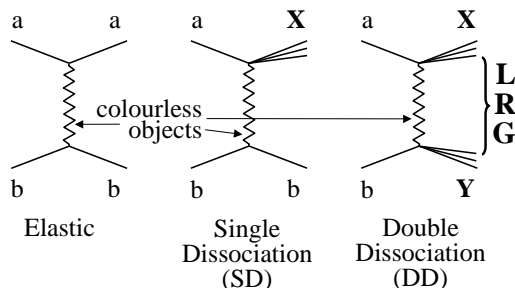


Figure 1. Diagrams for the elastic (left), single dissociation (centre) and double dissociation (right) reactions.

### 1.1 Definition of diffractive scattering

From the experimental point of view, diffractive scattering can be defined as the sample of events ( $\sim 30\%$  of the total cross section) in which: *i*) the beam particles either remain intact (elastic) or dissociate into one or two hadronic systems (X, Y in Fig. 1) of mass  $M_{X,Y}^2$  much smaller than the centre-of-mass energy  $s$ ; *ii*) there is a  $t$ -channel colour-singlet exchange; *iii*) the emerging systems hadronise independently, producing a large rapidity gap (LRG) in the distribution of the final-state particles if the centre of mass energy  $s$  is large enough (for single dissociation  $y \approx \frac{1}{2} \cdot \ln \frac{s}{M_X^2}$ ). The experimental observations in diffractive hadronic scattering embrace a weak energy dependence of the cross section ( $\sigma \propto s^{0.16}$ ), very small scattering angles (parameterised by an exponential dependence of  $t$ , the square of the four-momentum exchanged,  $e^{-b(s) \cdot |t|}$ ) and  $t$ -slopes,  $b$ , which are measured to depend on  $\ln(s)$  (often called shrinkage, since it is manifest as a shrinkage of the forward ( $t = 0$ ) elastic peak with increasing  $s$ ).

## 2 The hadronic language: the Regge theory and the parameters $\alpha_{\mathbb{P}}(0)$ and $\alpha'_{\mathbb{P}}$

The experimental observations mentioned above are successfully described within the framework of the Regge theory. This is a

theory of scattering in the complex angular momentum plane, in which hadronic scattering is described by the exchange of collective states, called trajectories, which are made by families of particles whose spins are measured to be in linear relation with their squared masses at small values of  $|t|$ . This property allows one to parameterise the trajectories as  $\alpha_j(t) = \alpha_j(0) + \alpha'_j \cdot t$ , where  $j$  can be a pion, a pomeron ( $\mathbb{P}$ ) or a reggeon ( $\mathbb{R}$ ). As an example, the cross section for the elastic process  $ab \rightarrow ab$  can be written, for small  $|t|$ , in Regge theory as  $\frac{d\sigma_{el}^{ab}}{d|t|} = \frac{1}{16\pi} \cdot \sum_j [\beta_{aj}(0) \cdot \beta_{bj}(0)]^2 \cdot s^{2(\alpha_j(0)-1)} \cdot e^{-b(s) \cdot |t|}$ , where the (“residue”) functions  $\beta(t)$  represent the couplings,  $b(s) = b_a + b_b + 2\alpha'_j \cdot \ln(s)$  and  $b_a$  and  $b_b$  originate from the form factors of the hadrons  $a$  and  $b$ . The formula for  $\frac{d\sigma_{el}^{ab}}{d|t|}$  describes the  $s$  and  $t$  dependence noted in Sect. 1.1

The  $\mathbb{P}$  trajectory<sup>a</sup> was postulated with an intercept  $\alpha_{\mathbb{P}}(0)$  larger than 1 to fit the hadronic total cross sections which increase at high energy. The simultaneous use of the  $\mathbb{P}$  and  $\mathbb{R}$  trajectories fitted the  $s$  dependence of the total cross section in  $pp, \pi p, Kp$  and  $\gamma p$  scattering using the simple form  $\sigma_{tot} = X \cdot s^{\alpha_{\mathbb{P}}(0)-1} + Y \cdot s^{\alpha_{\mathbb{R}}(0)-1}$ , where  $X$  and  $Y$  are constants. The values  $\alpha_{\mathbb{P}}(0) = 1.08$  and  $\alpha'_{\mathbb{P}} = 0.25$  obtained by the fits of Donnachie and Landshoff<sup>3</sup>, are often referred to as the *soft*  $\mathbb{P}$ . The fact that the high-energy behaviour of all the measured hadronic total cross sections could be described by the same  $\alpha_{\mathbb{P}}(0)$  is a great success for Regge phenomenology and shows that these two parameters are not just incidental parameters obtained by a phenomenological fit, but they have a deeper meaning. Indeed, they must be fundamental, since they represent uni-

<sup>a</sup>The  $\mathbb{P}$  trajectory carries quantum numbers  $C = P = +1$ . When it was introduced, it was the only one not associated with any real particle. Since then, the effort to find particles associated to the  $\mathbb{P}$  trajectory, the so called *glueballs*, has been continuous. Today's situation is reviewed in ref. <sup>2</sup>.

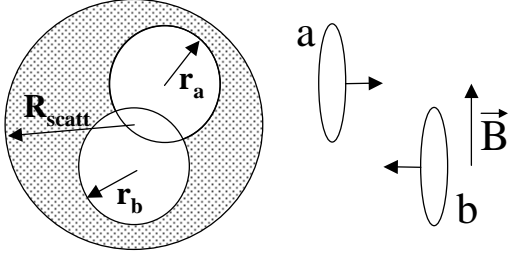


Figure 2. Cartoon of hadronic scattering in the transverse (left) and longitudinal (right) plane.

versal (i.e. independent of the initial state hadrons) features of the strong forces that govern the binding of hadrons<sup>4</sup>. The *intercept*  $\alpha_{\mathbb{P}}(0) = 1 + \epsilon$  governs the energy dependence of the total ( $\sigma_{tot} \propto s^\epsilon$ ), elastic and diffractive ( $\sigma_{el}, \sigma_{diff} \propto s^{2\epsilon}$ ) cross sections. Therefore, in a geometrical interpretation, it can be related to the transverse extension of the scattering system ( $R_{scatt}$  in Fig. 2 left), i.e. of the colour-radiation cloud, which increases with energy. The *slope*  $\alpha'_{\mathbb{P}}$  on the other hand determines the dependence of the cross section on the impact parameter  $\vec{B}$  (Fig. 2 right),  $\langle \vec{B}^2 \rangle = 2b(s) = 2[b_a + b_b + 2\alpha'_{\mathbb{P}} \cdot \ln(s)]$  as described in <sup>4</sup>. As such,  $\alpha'_{\mathbb{P}}$  reflects the strength of the binding forces and characterizes the confinement forces in QCD. It is important to stress here that only diffractive interactions give access  $\alpha'_{\mathbb{P}}$ , since its measurement requires semi-inclusive diffractive processes in order to measure  $t$ .

The calculation of  $\alpha_{\mathbb{P}}(0)$  and  $\alpha'_{\mathbb{P}}$  from first principles is of primary importance. Many efforts have been going on in recent years, based on novel physical concepts and mathematical methods. As an example, Kharzeev et al.<sup>5</sup> introduced a new type of instanton-induced interaction (instanton ladder) which is proposed to be responsible for the structure of the soft  $\mathbb{P}$ . The work by Witten<sup>6</sup>, in which confinement and mass gap (but not asymptotic freedom and mass spectra) are obtained in the framework of string theory, shows how diverse and basic are the

attempts to go beyond pQCD.

### 3 The partonic language: hard diffraction and QCD

So far, we discussed soft-hadronic interactions, which are governed by the hadronic degrees of freedom. However, to understand the dynamics, we need to describe hadronic phenomena in terms of hadron sub-components and quantum-field theories, i.e. in terms of partons and QCD. Since we are able to apply perturbative methods to QCD only if a hard scale is present, the theory is currently limited to the calculation of hard interactions. As we will see in this Section, there are two approaches to diffraction in the presence of a hard scale, which have their interpretation in different reference frames. But, before discussing the theory of hard diffraction, let us review the advantages that HERA offers to this field.

#### 3.1 Diffractive scattering at HERA

The HERA collider at DESY, born to study the proton structure functions and to search for exotic processes, acquired a central rôle in the attempt to understand diffractive interactions. There are several advantages in studying diffractive hard scattering at HERA. Deep-inelastic scattering (DIS) is much simpler than hadron-hadron collisions, since only one hadron, i.e. one large ( $\sim 1$  fm) non-perturbative object, is present in the initial state. The huge range in resolution power,  $0 < Q^2 < 10^5$  GeV<sup>2</sup> ( $Q^2$  is the negative squared four momentum of the exchanged virtual photon,  $\gamma^*$ ), which corresponds to probing distances of  $10^{-3} < \Delta r < 1$  fm, allows the investigation of both the short and long distance regions. The small- $x$  values reachable at HERA, where  $x$  is the Bjorken DIS scaling variable, correspond to a region of high parton densities; thus information on the saturation (and possibly confinement) of the partons in the proton might be accessed. The

asymmetric beam energies ( $E_e = 27.5$  GeV and  $E_p = 820$  or  $920$  GeV) offer an excellent experimental acceptance for the  $\gamma$ -diffractively-dissociated system, thus opening up the photon hemisphere. Finally, about 10% of the DIS events at small- $x$  at HERA are diffractive, providing large samples of events to study.

It is important to mention that the universality of  $\alpha_{\mathbb{P}}(0)$  and  $\alpha'_{\mathbb{P}}$  experimentally holds as long as we consider the scattering between hadrons. At HERA, where a virtual photon emitted by the beam lepton scatters off a proton, the measured IP trajectory<sup>b</sup> is found to depend on the photon virtuality<sup>7</sup> or on the diffractive final state<sup>8,9</sup>. This result is expected<sup>4</sup> to provide information, otherwise inaccessible, on the dynamics of strong interactions.

### 3.2 The diffractive structure functions

The cross section for the diffractive process  $ep \rightarrow eXp$  in DIS can be written:

$$\frac{d^4\sigma_{diff}}{d\beta dQ^2 dx_{\mathbb{P}} dt} = \frac{2\pi\alpha^2}{\beta Q^4} (1 + (1 - y)^2) F_2^{D(4)}(\beta, Q^2, x_{\mathbb{P}}, t),$$

where  $\alpha$  is the electromagnetic coupling constant,  $y$  the inelasticity and the contributions of the longitudinal proton structure function and of  $Z^0$  exchange have been neglected. The diffractive structure function  $F_2^{D(4)}$  depends on four variables. As can be seen in Fig. 3, in first approximation,  $Q^2$  and  $\beta$  describe the photon vertex while  $x_{\mathbb{P}}$  and  $t$  describe the proton vertex. In a reference frame in which the proton is fast, Breit or Bjorken-DIS frames (*DIS picture*),  $\beta = \frac{Q^2}{M_X^2 + Q^2}$  can

<sup>b</sup>Even if it is still possible to use the IP language in diffractive hard scattering, there are models which do not make use of the concept of IP. In the following, I will continue to use the term “IP”, but the reader should remember that this will not be the soft IP we discussed in Section 2.

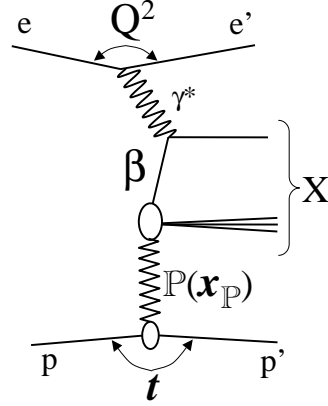


Figure 3. Schematic view of diffractive deep inelastic  $ep$  scattering.

be identified with the fraction of the IP momentum carried by the quark which couples to the  $\gamma^*$  and  $x_{\mathbb{P}} = \frac{M_X^2 + Q^2}{W^2 + Q^2}$  with the fraction of the proton momentum carried by the IP. In the previous formula,  $W$  is the  $\gamma p$  centre of mass energy. Integration over  $t$  gives  $F_2^{D(3)}(\beta, Q^2, x_{\mathbb{P}})$ .

### 3.3 Models for hard diffraction

The era of hard diffraction started in 1987, when the UA8 collaboration at the SPSC measured diffractive jet production in  $p\bar{p}$  scattering<sup>10</sup>. This process was predicted by Ingelman and Schlein<sup>11</sup> a few years earlier, in the framework of a model in which the concept of the soft IP was applied to hard diffractive scattering. The Ingelman-Schlein model was based on several assumptions. It was assumed that the soft IP has a partonic structure like a real hadron, that Regge factorisation holds, i.e. that the diffractive structure function can be factorised into  $F_2^{D(4)}(\beta, Q^2, x_{\mathbb{P}}, t) = \Phi_{\mathbb{P}/p}(x_{\mathbb{P}}, t) \cdot F_2^{D(2)}(\beta, Q^2)$ , and that the IP flux is the one given by Regge theory,  $\Phi_{\mathbb{P}/p}(x_{\mathbb{P}}, t) = (1/x_{\mathbb{P}})^{2\alpha_{\mathbb{P}}(t)-1}$ .

In recent years there has been a lot of progress in the theory of diffractive DIS. Hard

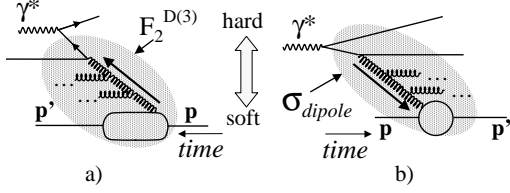


Figure 4. Comparison between the DIS (a) and the dipole (b) pictures.

QCD factorisation:

$$\frac{d^4 \sigma_{diff}}{d\beta dQ^2 dx_{\mathbb{P}} dt} = \sum_i \int_x^{x_{\mathbb{P}}} dx' \hat{\sigma}_{hard}(x, Q^2, x') \cdot \frac{df_i^D(x', x_{\mathbb{P}}, t)}{dx_{\mathbb{P}} dt}$$

was proven<sup>12</sup> for large enough  $Q^2$ . Here  $\hat{\sigma}_{hard}$  is the partonic hard cross section. The non-perturbative diffractive parton distributions<sup>13</sup> (DPD's)  $\frac{df_i^D(x', x_{\mathbb{P}}, t)}{dx_{\mathbb{P}} dt}$  are conditional probabilities of finding, in a fast proton, a parton  $i$  with longitudinal momentum fraction  $x'$ , while at the same time the beam proton is scattered with  $t$  and  $(1 - x_{\mathbb{P}})$ . DPD's were also found to obey the usual DGLAP evolution equations<sup>12</sup>. These results allow the assertion that, like inclusive DIS, diffractive DIS is firmly rooted in QCD.

In a frame where the proton is fast, diffractive DIS can be described as follows (see Fig. 4a). A parton is emitted by the fast proton and then evolves into a parton cascade which eventually produces a  $q\bar{q}$  pair that interacts with the  $\gamma^*$ . The parton emission in this frame is ordered in time from the proton to the  $\gamma^*$  side. The presence of a hard scale solves only part of the problem by making the upper part of the diagram in Fig. 4a calculable in pQCD, while the lower, soft part of the interaction, parameterized by the DPD's, occurs over a large space-time and a perturbative treatment is not possible.

The physical picture of diffractive DIS is most easily seen in models built in the proton rest frame (Fig. 4b). In this frame, the  $\gamma^*$  fluctuates into a  $q\bar{q}$  ( $q\bar{q}g, \dots$ ) system of life-

time  $\tau \approx 1/x$ . At the small- $x$  values available at HERA, this lifetime corresponds to a large distance, up to 1000 fm. Thus, from the point of view of the proton, the  $q\bar{q}$  system is frozen and the interaction happens between a colour dipole and the proton. As a consequence, these models are named *dipole models*. The diffractive cross section in the target frame can be written:

$$\sigma = \int d^2r dz \cdot |\psi(r, z, Q^2)|^2 \cdot \sigma_{dipole}^2(x, r)$$

where  $\psi$  is the  $\gamma^* \rightarrow q\bar{q}$  wave function,  $z$  is the fraction of the  $\gamma^*$  momentum carried by one of the quarks and  $r$  is the dipole size, i.e. the transverse separation of the  $q\bar{q}$  system. The non-perturbative structure is contained in the dipole cross section,  $\sigma_{dipole}$ , which is modelled at the lowest order in pQCD by a two-gluon exchange. The time ordering of the parton emissions in the target frame is reversed with respect to the DIS frame: in the target frame, the  $\gamma^*$  fluctuates into a  $q\bar{q}$  colour dipole which develops a parton cascade and finally interacts with the proton.

It should be noted that, despite the apparent differences between the two approaches to DIS, the physics must be the same. A theoretical effort<sup>14</sup> is indeed going on, to establish a correspondence between NLO and large  $r^2$  in the two approaches.

#### 4 Structure functions and jet measurements in diffractive DIS

Three different methods are used to identify diffractive events at HERA: *i*) the scattered proton is measured in spectrometers positioned along the proton beamline, such as the ZEUS LPS<sup>15</sup> and the H1 FPS<sup>16</sup>; *ii*) a LRG in the final state is required in the direction of the outgoing proton. This is achieved<sup>17</sup> by requiring no energy deposits above a certain threshold (e.g. 400 MeV) at pseudorapidities smaller than a value  $\eta_{max}$ , thus imposing no-hadronic activity around the scattered proton; *iii*) the diffractive sample is sepa-

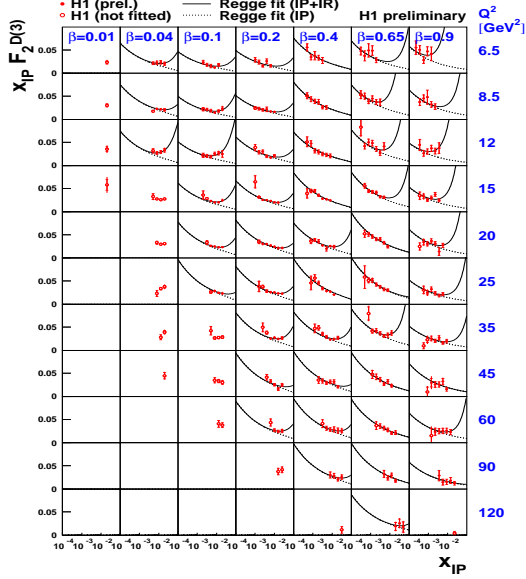


Figure 5.  $x_{\mathbb{P}} F_2^{D(3)}$  vs.  $x_{\mathbb{P}}$  at fixed values of  $\beta$  and  $Q^2$ . The lines show the results of the fit described in the text (full lines:  $\mathbb{IP} + \mathbb{IR}$ , dotted lines:  $\mathbb{IP}$  only). Open symbols indicate the points excluded from the fit.

rated from the non-diffractive events by using the fact that the non-diffractive sample has an exponentially falling dependence on  $M_X^2$ , while the diffractive part has an approximate  $1/M_X^2$  dependence<sup>18</sup>.

#### 4.1 $F_2^D$ measurements

A new, high-precision measurement<sup>19</sup> of the diffractive structure function  $F_2^{D(3)}$  was performed by the H1 Collaboration in the kinematic range  $6.5 < Q^2 < 120 \text{ GeV}^2$ ,  $0.01 < \beta < 0.9$ ,  $10^{-4} < x_{\mathbb{P}} < 0.05$  and  $|t| < 1 \text{ GeV}^2$ . The event selection requires a LRG in the final state, thus selecting  $ep \rightarrow eXY$  events, where  $Y$  is either a proton or a low-mass proton-excitation system. The  $x_{\mathbb{P}}$  dependence of the data is well described by Regge phenomenology (see Fig. 5) if a leading ( $\mathbb{IP}$ ) and a secondary ( $\mathbb{IR}$ ) trajectory exchanges are assumed. The effective pomeron

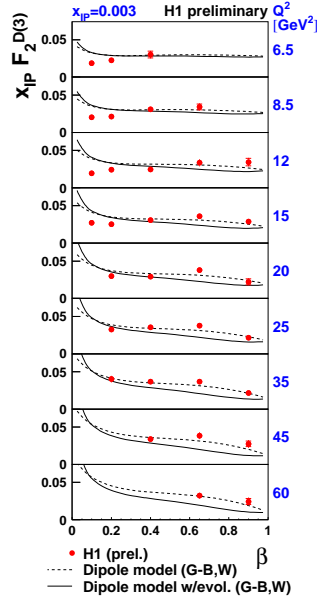


Figure 6.  $x_{\mathbb{P}} F_2^{D(3)}$  at fixed  $x_{\mathbb{P}} = 0.03$  as a function of  $\beta$  for various values of  $Q^2$ . The lines show the prediction of the saturation model without<sup>20</sup> (dashed lines) and with<sup>21</sup> (full lines) QCD DGLAP evolution.

intercept is measured to be  $\alpha_{\mathbb{P}}(0) = 1.173 \pm 0.018(\text{stat.}) \pm 0.017(\text{syst.})^{+0.063}_{-0.035}(\text{model})$ . The ratio  $\sigma_{\text{diff}}/\sigma_{\text{tot}}$  is relatively flat as a function of  $W$ . The data are well described by a fit based on the DGLAP evolution of the  $\beta$  and  $Q^2$  dependence and Regge factorisation, with a Regge motivated  $(1/x_{\mathbb{P}})^{2\alpha_{\mathbb{P}}(t)-1}$  dependence.

In Fig. 6, the H1 data are compared with two versions of the “saturation” model by Golec-Biernat and Wüsthoff<sup>20,21</sup>. In this model, the unitarity of  $\sigma_{\text{dipole}}$  at small  $x$ , that is the fact that the cross sections should not diverge at asymptotic energies as it happens in the QCD description based on linear evolution equations, is imposed. Unitarity is built by postulating the phenomenological form

$$\sigma_{\text{dipole}} = \sigma_0 \cdot [1 - \exp(-\frac{r^2}{4R_0(x)^2})],$$

where  $R_0(x) = \frac{1}{Q_0} \cdot (\frac{x}{x_0})^{\frac{1}{\lambda}}$  can be interpreted as the saturation radius,  $Q_0 = 1 \text{ GeV}$ , and  $\sigma_0$ ,  $x_0$  and  $\lambda$  are free parameters of the

model. At small  $r$ , the dipole cross section exhibits colour transparency ( $\sigma_{dipole} \approx r^2$ ), which is a purely pQCD phenomenon, while saturation ( $\sigma_{dipole} \simeq \sigma_0$ ) occurs at large  $r$ . The transition between the two regimes is governed by the saturation radius  $R_0(x)$ . The saturation model contains a higher-twist contribution at large  $\beta$ , which allows comparisons to be made throughout the full measured kinematic region. The values of the three parameters  $\sigma_0$ ,  $x_0$  and  $\lambda$  obtained by a fit to inclusive DIS data with  $x < 0.01$ , were used to predict  $F_2^D$ . The result, shown in Fig. 6, gives a good description of the data except at small  $\beta$  and  $Q^2$ . The model in which QCD DGLAP evolution is added<sup>21</sup> (full lines in Fig. 6) underestimates the measured  $F_2^{D(3)}$  at high  $\beta$  and  $Q^2$ .

The H1 data were also compared with the “*semi-classical*” model by Buchmüller et al.<sup>22</sup>. In this model, the proton is seen as a superposition of soft colour fields parameterised according to a simple non-perturbative model that averages over all field configurations. In the target frame, the  $q\bar{q}$  or  $q\bar{q}g$  fluctuations of the  $\gamma^*$ , modelled as colour dipoles, traverse the proton colour field. Diffractive (non-diffractive) interactions occur if both colour dipole and target emerge in a colour singlet (octet) state<sup>c</sup>. The model, which contains only four parameters obtained by a combined fit to the  $F_2$  and  $F_2^D$  data, reproduces the general features of the data<sup>19</sup> (not shown) but lies above the data when  $\beta$  and  $Q^2$  are both small.

The process  $ep \rightarrow eXp$  has been studied<sup>23</sup> by the ZEUS Collaboration selecting diffractive events by the requirement of a scattered proton track, carrying a fraction of the initial proton momentum  $x_L > 0.95$ , in the ZEUS leading proton spectrometer (LPS). The detection of the final state proton in the LPS (though substantially reduced the

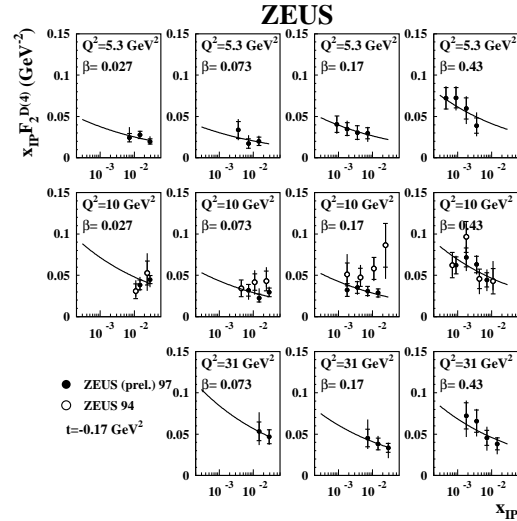


Figure 7. ZEUS LPS measurement of  $x_P F_2^{D(4)}$  (solid points) as a function of  $x_P$  for the  $\beta$ ,  $Q^2$  and  $t$  values indicated in the plot. Solid lines show the result of the fit described in <sup>23</sup>. Open points show the results obtained in the previous ZEUS LPS measurement<sup>24</sup>.

event sample because of the small LPS acceptance) allows a direct measurement of  $t$ . It also provides the cleanest selection of diffractive events, independent of the hadronic final state and free of the proton-dissociation background events,  $ep \rightarrow eXY$ . The diffractive structure functions  $F_2^{D(3)}$  and  $F_2^{D(4)}$  were measured in the kinematic range  $4 < Q^2 < 100 \text{ GeV}^2$ ,  $0.01 < \beta < 0.6$ ,  $10^{-4} < x_P < 0.04$  and  $0.075 < |t| < 0.035 \text{ GeV}^2$ . Figure 7 shows the measured  $x_P F_2^{D(4)}(\beta, Q^2, x_P, t)$  as a function of  $x_P$  for different values of  $\beta$  and  $Q^2$  and for average  $t = -0.17 \text{ GeV}^2$ . The  $x_P$  dependence of the  $F_2^{D(3)}$  obtained with the LPS can be fitted using a flux factor  $(1/x_P)^{2\alpha_P(t)-1}$  (solid lines in Fig. 7), therefore showing consistency with Regge factorisation. The value of the pomeron intercept obtained by this fit is  $\alpha_P(0) = 1.13 \pm 0.03(\text{stat.})^{+0.03}_{-0.01}(\text{syst.})$ .

<sup>c</sup>This model is particularly interesting since it made the prediction  $\sigma_{diff}/\sigma_{tot} \approx$  independent of  $W$ , which is found in the data<sup>18,19</sup>.

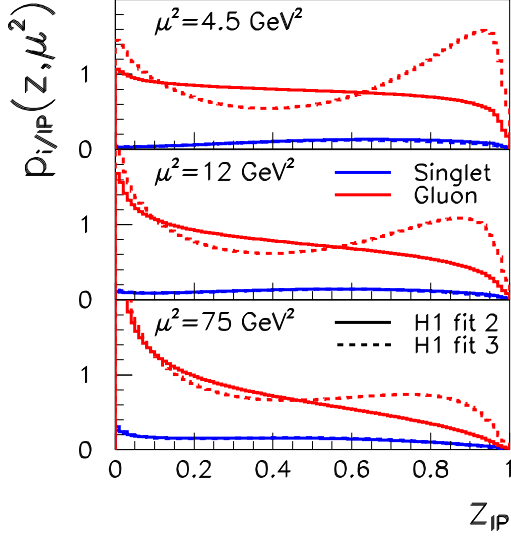


Figure 8. The quark and gluon distributions extracted at various values of  $Q^2$  for two different parameterisations of the parton densities.

#### 4.2 Extraction of DPD's from inclusive diffraction

H1 extracted the DPD's from inclusive diffractive data<sup>25</sup>. They used a QCD-motivated model in which parton distributions, which evolve according to the NLO DGLAP evolution equations, are assigned to the leading (IP) and subleading (IR) exchanges utilized to parameterise the data. Under such a hypothesis, the data require approximately 90% and 80% of the momentum of the pomeron to be carried by gluons at  $Q^2 = 4.5 \text{ GeV}^2$  and  $Q^2 = 75 \text{ GeV}^2$ , respectively (see Fig. 8). The inclusive measurements are not particularly sensitive to the shape of the gluon distribution at large  $z_{\text{IP}}$ , the momentum fraction of partons in the pomeron<sup>d</sup>, and both the “flat gluon” (full lines in Fig. 8) and the “peaked gluon” (dashed lines in Fig. 8) fits give a good  $\chi^2$ .

<sup>d</sup>Notice that  $z_{\text{IP}} \equiv \beta$  if the parton in the IP is a quark.

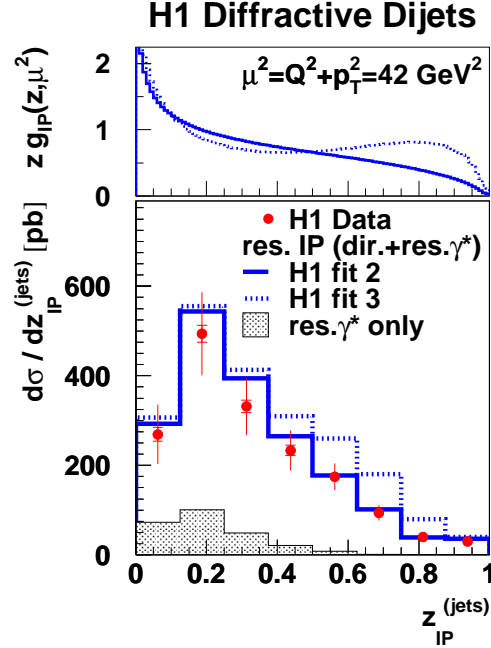


Figure 9. The diffractive dijet cross section as a function of  $z_{\text{IP}}$ . The data are compared to the results obtained by the RAPGAP Monte Carlo (MC) using the “flat gluon” (solid line) and the “peaked gluon” (dotted line) from the H1 QCD fit<sup>25</sup>. The corresponding gluon distributions are shown on the top plot.

#### 4.3 Diffractive jet production

Diffractive dijet production shows higher sensitivity to the gluon density in the IP than the inclusive measurements. The dijet cross sections have been measured<sup>26</sup> by H1 in the kinematic range  $4 < Q^2 < 80 \text{ GeV}^2$ ,  $90 < W < 260 \text{ GeV}$ ,  $23 < M_X < 40 \text{ GeV}$  and  $x_{\text{IP}} < 0.05$  for jets of  $p_T > 4 \text{ GeV}$  reconstructed using the cone algorithm ( $R = 1$ ) in the  $\gamma^*p$  reference frame. The H1 cross sections, compared in Fig. 9 to the RAPGAP<sup>27</sup> MC, which is an implementation of the Ingelman-Schlein model, favour the flat-gluon DPD's. The dijet cross sections in bins of  $Q^2 + p_T^2$  and  $x_{\text{IP}}$  show<sup>26</sup> that the DGLAP evolution holds and that the data are consistent with Regge factorisation, respectively, as assumed in the RAPGAP MC.

ZEUS measured<sup>28</sup> diffractive three-jet



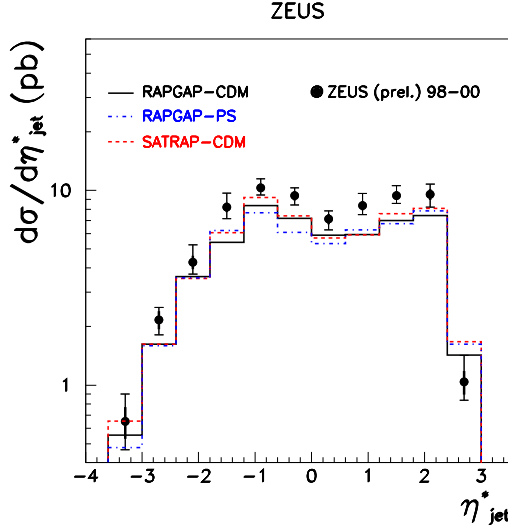


Figure 10. The diffractive cross section for three jet events as a function of the pseudorapidity in the  $\gamma^*\text{IP}$  frame of each jet,  $\eta_{jet}^*$ .

cross sections in the kinematic range  $5 < Q^2 < 100 \text{ GeV}^2$ ,  $200 < W < 250 \text{ GeV}$  and  $23 < M_X < 40 \text{ GeV}$ . The jets were reconstructed using the  $k_T$  algorithm in the  $\gamma^*\text{IP}$  reference frame. The result, shown in Fig. 10, is broadly consistent with models in which the hadronic final-state is dominated by a  $q\bar{q}g$  system with the gluon preferentially emitted in the pomeron direction. Such configurations are predicted both by RAPGAP and by the SATRAP<sup>29</sup> MC, which is based on the saturation model. The two MC models describe the data equally well, except for a ( $\approx 20\%$ ) normalisation factor, which can probably be ascribed to higher order corrections that are only included approximately by parton showers.

## 5 Universality of the DPD's?

The CDF Collaboration measured the diffractive structure functions from dijet events,  $F_{jj}^D(\beta)$ , in  $p\bar{p}$  collisions at the Tevatron. The results<sup>30</sup>, shown in Fig. 11, are a factor of ten smaller than the predictions for  $p\bar{p}$  interactions obtained using the DPD's measured at HERA (two upper curves in

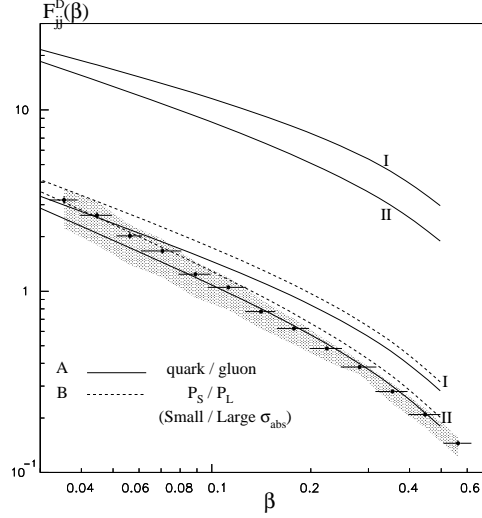


Figure 11. The CDF measurement of  $F_{jj}^D(\beta)$  (black circles) compared with predictions<sup>31</sup> obtained for two sets of HERA DPD's (I and II). The upper two curves correspond to the neglect of rescattering corrections, whereas the lower four curves show the effect of including these corrections using two models (A and B) for the diffractive eigenstates.

Fig. 11). Breakdown of vertex factorisation between  $ep$  and  $p\bar{p}$  interactions was advocated to explain this result. The concept of LRG survival probability, which accounts for the possibility of secondary emissions which might fill with particles the LRG in the final state of diffractive events, was recently revived. This concept follows and complements the line of studies on rescattering corrections in hadronic interactions (see references in <sup>31</sup>). Recently, Kaidalov et al.<sup>31</sup> made a parameter-free computation of the LRG survival probability using ISR and Tevatron soft scattering data. The  $F_{jj}^D(\beta)$  they obtained using the LRG survival probability they computed, together with the HERA DPD's, is in surprising agreement with the CDF data (four bottom curves in Fig. 11). The uncertainty in the calculation is dominated by the uncertainty in the IP structure functions. This result supports the universality of DPD's.

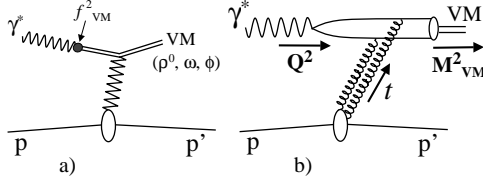


Figure 12. Diagrams for elastic VM scattering at HERA,  $ep \rightarrow eVp$ : a) soft VM production, b) hard VM production.

## 6 Exclusive production of vector mesons at HERA

The exclusive (or elastic) production of vector mesons (VM) at HERA ( $ep \rightarrow eVp$ , where  $V = \rho^0, \omega, \phi, J/\psi, \psi'$  or  $\Upsilon$ ) is a very clean experimental process. As it is measured in a wide kinematic range,  $0 < Q^2 < 100 \text{ GeV}^2$ ,  $20 < W < 290 \text{ GeV}$ ,  $0 < |t| < 20 \text{ GeV}^2$ , it constitutes an important process to study the dynamics of strong interactions and allows simultaneous control of the possible hard scales,  $Q^2$ ,  $t$  or the squared VM mass  $M_{VM}^2$ .

The elastic photoproduction ( $Q^2 \approx 0$ ) of light VM ( $\rho^0, \omega, \phi$ ) is measured<sup>32</sup> to be a soft process, since it shows the properties typical of soft diffraction (see Sect. 1.1). It can be described by the Vector Dominance Model and the Regge theory. In this framework, the photon fluctuates into a VM prior to the interaction, followed by an elastic  $Vp \rightarrow Vp$  scatter, as shown in Fig. 12a. The picture becomes quite different if a hard scale is present, and therefore pQCD is expected to be applicable. In this case, the elastic VM production can be seen as a three-step process (see Fig. 12b): in the target frame, the  $\gamma^*$  fluctuates into a  $q\bar{q}$  dipole, which then scatters off the proton by a colour-singlet two-gluon exchange (at the lowest order), and finally the VM is formed, well after the interaction. If the dipole size  $r = 1/\sqrt{z(1-z)Q^2 + m_q^2}$  is small, i.e. we are either in the presence of a large quark mass  $m_q$  or of a longitudinal  $\gamma^*$  of high virtuality, the  $q\bar{q}$  pair is

able to resolve the gluons in the proton, and thus pQCD is applicable. In this case, the cross section is expected to behave in a different way than in soft diffraction. Indeed, pQCD calculations<sup>33</sup> for longitudinal photons predict: *i*) a fast rise with energy,  $\sigma_L \propto [1/Q^6] \cdot \alpha_s^2(Q_{eff}^2) \cdot [xg(x, Q_{eff}^2)]^2 \propto W^{0.8}$ , since  $xg(x, Q_{eff}^2)$  is measured at HERA to be  $\approx x^{-0.2}$  and  $x \approx 1/W^2$  at small  $x$ ; *ii*) a tendency to approach the universality of the  $t$ -dependence, namely  $d\sigma/dt \propto e^{-b_{2g}|t|}$ , with  $b_{2g} \sim 4 \text{ GeV}^{-2}$ , almost independent of  $W$  (i.e.  $\alpha'_P \rightarrow 0 \Rightarrow$  small shrinkage); *iii*) an approximate restoration of flavour independence, i.e. the  $\gamma^*$  couples directly to the constituent quarks and the  $\rho^0 : \omega : \phi : J/\psi$  ratios are expected to converge to the *modified* SU(4) ratios  $9 : 1 \cdot 0.8 : 2 \cdot 1.2 : 8 \cdot 3.5$  when the hard scale  $Q_{eff}^2$  is large enough that the VM wave functions converge to an asymptotic form<sup>33</sup>.

It is important to verify if these predictions are supported by the data. It is also interesting to investigate at which scale the  $xg(x, Q_{eff}^2)$  should be evaluated, i.e. which or which combination of  $Q^2$ ,  $t$  and  $M_{VM}^2$  enter in  $Q_{eff}^2$ .

### 6.1 The HERA measurements

The elastic process  $ep \rightarrow eVp$  has been extensively studied at HERA for many years. One of the earliest results was the determination in photoproduction of the  $W^{\sim 0.22}$  dependence<sup>32</sup> for light VM's ( $\rho^0, \omega$  and  $\phi$ ) while the  $J/\psi$  dependence<sup>32</sup> was more like  $W^{0.8}$ . The behaviour of  $\sigma_{\gamma p \rightarrow J/\psi p}$  at  $Q^2 \approx 0$ , is described by the model of Ryskin<sup>34</sup> when the steep gluon density measured at HERA is used. This result shows that the  $J/\psi$  mass provides a hard enough scale to apply pQCD even in photoproduction. ZEUS measured<sup>8,9</sup> the double differential elastic cross sections as a function of  $W$  and  $t$  for  $\rho^0, \phi$  and  $J/\psi$  photoproduction. By fitting the  $W$  dependence in the  $t$  bins, the pomeron trajectories

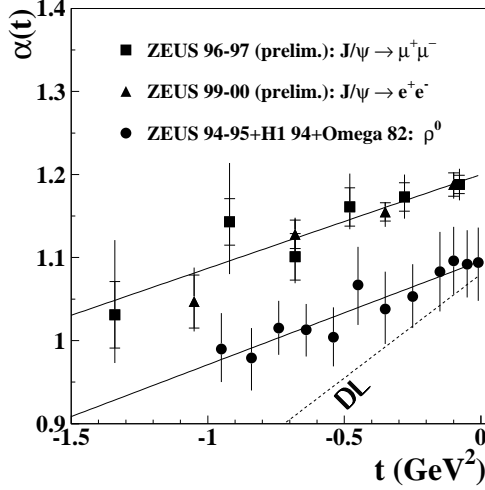


Figure 13. Pomeron trajectories extracted from elastic photoproduction of  $\rho^0$  and  $J/\psi$  mesons. The dashed line marked DL shows the soft IP trajectory<sup>3</sup>.

Table 1. Pomeron trajectories: the first three entries refer to photoproduction and the fourth to DIS. For comparison, the DL soft pomeron<sup>3</sup> is also listed.

	$\alpha_{\mathbb{P}}(0)$	$\alpha'_{\mathbb{P}} [\text{GeV}]^{-2}$
$\rho^0$	$1.096 \pm 0.021$	$0.125 \pm 0.038$
$\phi$	$1.081 \pm 0.010$	$0.158 \pm 0.028$
$J/\psi$	$1.198 \pm 0.012$	$0.114 \pm 0.025$
$\rho^0(\text{DIS})$	$1.14 \pm 0.03$	$0.04^{+0.15}_{-0.08}$
DL soft	1.08	0.25

responsible for the production of the different VM's can be extracted. The results, shown in Fig. 13 and Table 1, show that, when extracted this way, the measured IP trajectory is not universal. In particular, in the case of the  $J/\psi$  both  $\alpha_{\mathbb{P}}(0)$  and  $\alpha'_{\mathbb{P}}$  support the pQCD predictions *i*) and *ii*) of Sect. 6.

The ZEUS measurement<sup>7</sup> of the  $ep \rightarrow e\rho^0 p$  deep-inelastic cross sections as a function of  $W$  in bins of  $Q^2$  from  $Q^2 \approx 0$  to  $Q^2 = 27 \text{ GeV}^2$  are shown in Fig. 14. A fit to  $\sigma_{ep \rightarrow e\rho^0 p}$  with a  $W^\delta$  dependence shows that, within the  $Q^2$  range measured,  $\delta$  varies from  $\delta = 0.16 \pm 0.06$  typical of soft scattering to  $\delta = 0.88 \pm 0.22$ , close to the value found in

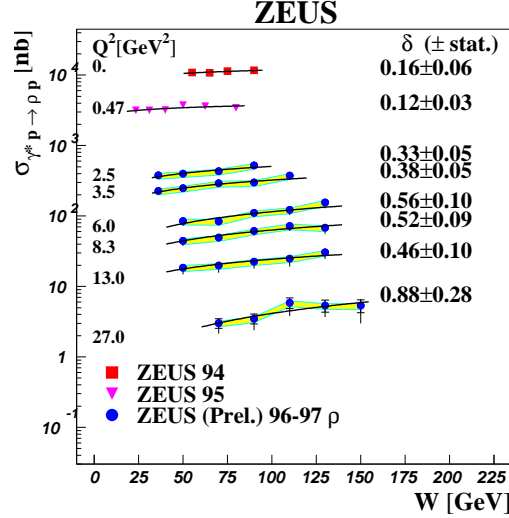


Figure 14. Elastic  $\rho^0$  cross sections vs.  $W$  for several values of  $Q^2$ . The results of the fits in the various  $Q^2$  bins with a  $W^\delta$  dependence are shown.

the case of  $J/\psi$  photoproduction. This transition from the soft to the hard regime proves that also large values of  $Q^2$  provide a hard scale to apply pQCD to elastic VM production at HERA. The result of the extraction of the pomeron trajectory from these data is also shown in Table 1. Though statistically limited, there is a hint that the pomeron trajectory extracted from  $\rho^0$  in DIS is closer to the one from  $J/\psi$  in photoproduction than to the soft DL one.

An early prediction of pQCD is a different  $Q^2$  dependence for the longitudinal ( $\sigma_L$ ) and transverse ( $\sigma_T$ ) cross sections. This prediction<sup>35</sup> was verified by plotting the ratio  $R = \sigma_L/\sigma_T$  as a function of  $Q^2$ ; the result<sup>7</sup> (not shown) is that  $R$  is found to increase with  $Q^2$  as expected in pQCD.

Another interesting quantity to study is the ratio of VM production cross sections. Fig. 15 shows that the  $\sigma_\phi/\sigma_\rho$  and  $\sigma_{J/\psi}/\sigma_\rho$  ratios for elastic scattering at HERA are measured to increase as a function of  $Q^2$ . In the case of  $\phi$  and  $\rho^0$ , the cross-section ratio approaches the asymptotic value given by the modified SU(4) factors, while in the

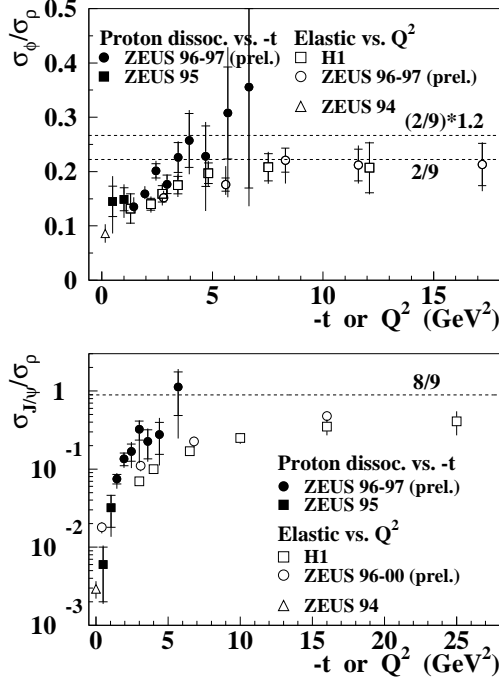


Figure 15. Ratio of  $\sigma_\phi/\sigma_\rho$  and  $\sigma_{J/\psi}/\sigma_\rho$  cross sections for elastic production vs.  $Q^2$  and for proton dissociative production vs.  $-t$ .

case of  $J/\psi$  and  $\rho^0$  the ratio is still rising at the largest  $Q^2$  measured, in agreement with pQCD predictions<sup>33</sup>. The ZEUS preliminary ratios for the proton dissociative cross sections  $ep \rightarrow eVY$  as a function of  $|t|$ , are also shown in Fig. 15. Remarkably, the data show that the ratios also rise with increasing  $|t|$ , which indicates that large values of  $|t|$  also constitute a hard scale, like  $Q^2$  and the VM mass. The faster rise with  $t$  than with  $Q^2$  of both ratios suggests that  $Q^2$  and  $t$  might not be equivalent scales, in the sense that the cross sections do not depend on them in the same way.

It was proposed<sup>36</sup> that the elastic VM cross sections might show a universal (i.e. independent of VM) behaviour vs. the variable  $Q^2 + M_{VM}^2$  after scaling the cross sections by the SU(4) factors 9 : 1 : 2 : 8. The new and more precise ZEUS data<sup>37</sup> (Fig. 16) show that, while the scaled  $\rho^0, \omega$  and  $\phi$  cross sec-

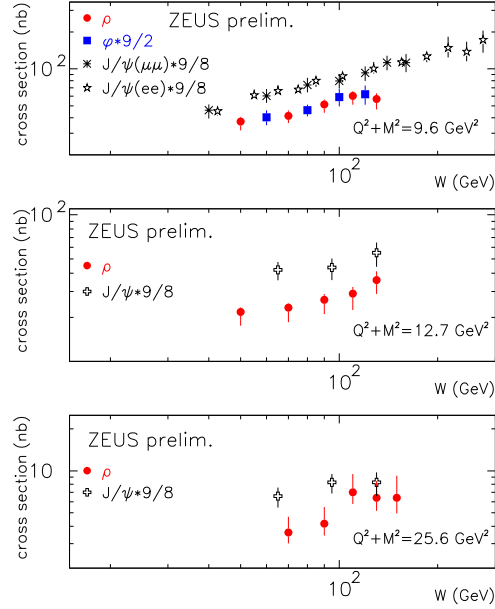


Figure 16. Comparison of scaled elastic VM cross sections at fixed  $Q^2 + M_{VM}^2$  values. The cross sections are weighted as indicated in the figure.

tions lie one on top of the other when plotted vs.  $Q^2 + M_{VM}^2$ , the scaled  $J/\psi$  cross sections are measured to be larger. The conclusion is that the behaviour advocated in<sup>36</sup> works for light VM production – when the VM masses are close to each other – but not for  $J/\psi$  production.

## 7 Selection of recent developments

### 7.1 Deeply virtual Compton scattering and generalised parton distributions

The deeply virtual Compton scattering (DVCS) is the exclusive production of a real photon in DIS,  $ep \rightarrow e\gamma p$ . This reaction, shown in Fig. 17, is similar to the elastic VM production, with the difference being that a real photon appears in the final state instead of a VM. Therefore the DVCS is theoretically simpler, since no VM wave function (a non-perturbative quantity) is in-

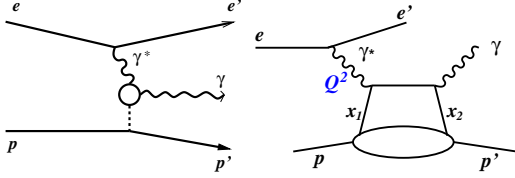


Figure 17. Left: generic diagram for DVCS. Right: one of the leading diagrams for DVCS in QCD.

volved. The DVCS process is considered particularly interesting since it gives access to the real part of the scattering amplitude and to the generalised parton distributions<sup>38</sup> (GPD's). The GPD's are fundamental quantities for exclusive processes in QCD since they unify the concepts of parton distributions and of hadronic form factors. Indeed, the blob in Fig. 17-left can be resolved at the lowest order in QCD into a two-parton exchange (e.g. Fig. 17-right) in which, to allow for  $t = (p - p')^2 \neq 0$ , the fractional transverse and longitudinal momenta of the two exchanged partons must be different<sup>e</sup>,  $k_{t1} \neq k_{t2}$  and  $x_1 \neq x_2$ . The usual parton distributions, for which  $x_1 = x_2 = x$ , are obtained from the squared wave functions for all partonic configurations containing a parton with the specified longitudinal momentum  $x$ , and therefore represent the probability to find such a parton. In contrast, the GPD's represent the interference of different wave functions, and thus correlate different parton configurations in the hadron at the quantum-mechanical level<sup>f</sup>. Therefore, in addition to the usual longitudinal momentum  $x$ , the GPD's account for parton  $k_T$  and two-particle correlations in the proton.

The DVCS process was searched for by H1<sup>39</sup> and ZEUS<sup>40</sup>. An excess of photons over

<sup>e</sup>The reader should notice that the condition  $t = (p - p')^2 \neq 0$  is in general true in diffractive scattering, and therefore GPD's should be used. However, most of the data shown so far are at small  $|t|$ , where the GPD's can be successfully approximated by the usual parton distributions.

<sup>f</sup>For this reason the GPD's are also called skewed or non-diagonal or off-forward parton distributions.

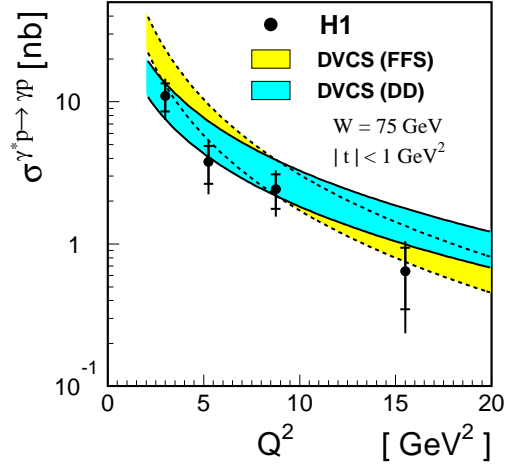


Figure 18. The DVCS cross section vs.  $Q^2$  compared to QCD-based calculations<sup>41,42</sup>.

the expectations of the QED-Compton background process was observed and the cross section for the DVCS process was measured as a function of  $W$  and  $Q^2$ . The results (see Fig. 18) are in agreement with the QCD-based predictions<sup>41,42</sup>.

## 7.2 Generalised parton distributions from inclusive diffraction at large $\beta$

Hebecker and Teubner suggested<sup>43</sup> that the generalised gluon distribution can be extracted from inclusive diffractive electroproduction at large  $Q^2$  and  $\beta \rightarrow 1$ . They demonstrated that, within certain restrictions in the kinematic domain, the process is, in principle, perturbatively calculable and highly sensitive to effects due to the non-diagonal parton distributions (skewing effects). A leading order numerical analysis, which includes corrections for the skewness of the parton distributions and for the real part of the amplitude, and an estimate of the NLO effects, is consistent with the  $F_2^D$  data (see Fig. 19). The results show the strong sensitivity of  $F_2^D$  to skewing effects, which amount to approximately a factor of two. Reversing the argument, they assert that precise data at higher  $Q^2$  and full NLO calculations should allow

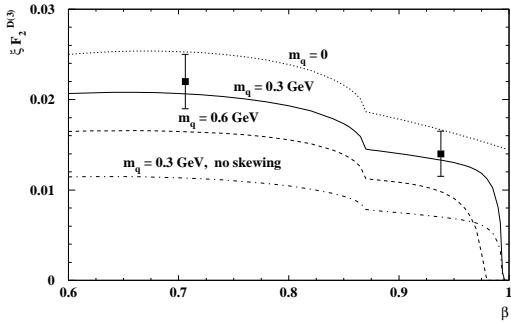


Figure 19.  $F_2^D$  at  $Q^2 = 60 \text{ GeV}^2$  and  $x_F = 0.0042$  for three different choices of the light quark mass as indicated in the plot. The ZEUS data<sup>18</sup> (squares) are also shown. The dash-dotted line is the prediction if the effects from skewing are neglected.

the extraction of GPD's with high accuracy.

### 7.3 Search for the odderon

In the framework of the Regge theory, it is possible to introduce a new trajectory, the  $C = P = -1$  partner of the pomeron trajectory, which would contribute with different signs to the particle-particle and particle-antiparticle total cross sections<sup>44</sup>. The exchange of this  $C$ -odd trajectory would therefore be responsible for any difference at asymptotic energies between these two total cross sections. For this reason, this hypothetical exchange was called odderon trajectory, from “odd-under-exchange”. No experimental sign of odderon exchange has been found in hadronic scattering.

QCD predicts the existence of the odderon, which can be represented at the lowest order by the exchange of three gluons, whereas the pomeron corresponds to the exchange of two gluons. Both perturbative QCD predictions<sup>45</sup> for the process  $\gamma p \rightarrow \eta_c p$  and non-perturbative QCD predictions<sup>46</sup> (based on the stochastic vacuum model) for the processes  $\gamma p \rightarrow \pi^0 X$  and  $\gamma p \rightarrow f_2(1270)X$  at HERA are available.

H1 made a search for odderon exchange by studying multi-photon final states in

diffractive events. This is an experimentally-clean QCD test with purely electromagnetic final states, except for the proton. Since the  $C$ -parity of the exchange fixes the number of photons in the final state, pomeron-mediated diffractive processes at HERA – such as  $\gamma p \rightarrow \omega p$  and  $\gamma p \rightarrow \omega \pi^0 X$  – have an even number of photons in the final state, while odderon-mediated diffractive processes – such as  $\gamma p \rightarrow \pi^0 X$ ,  $\gamma p \rightarrow f_2(1270)X$  and  $\gamma p \rightarrow a_2^0(1320)X$  – would manifest themselves by the presence of an odd number of photons in the final state. The result<sup>47</sup> is that, while signals are found for the pomeron-mediated processes and the measured cross sections are in agreement with previous measurements in other decay channels, no signal is found in any of the three odderon-mediated processes mentioned above.

## 8 Conclusions

It is not an easy task to draw conclusions on such a complicated topic such as diffractive scattering. For sure, the multitude of hard-diffraction studies at hadron colliders and at HERA and the huge theoretical effort to describe these phenomena in the framework of perturbative QCD, contributed to bridge between the hadronic –large distance– degrees of freedom typical of Regge theory and the partonic degrees of freedom which unveil the dynamics of strong interactions. An important piece is still missing, which should allow the description of large-distance processes within the framework of quantum-field theory. This is the field in which the study of diffractive phenomena is expected to provide useful data. Again, the problem turns into the understanding of the dynamics of colour radiation at large-distances, which is a long standing problem in QCD, that eventually coincides with the understanding of confinement of hadrons, one of the few remaining puzzles of the Standard Model of particle physics.

## Acknowledgments

I thank J. Bartels, T. Carli and J. Whitmore for their comments on an earlier version of this manuscript. I profited by the discussions with J. Bartels, W. Buchmüller, M. Diehl, K. Golec-Biernat, G.P. Vacca and by the forbearance of the ZEUS and H1 colleagues. I wish to express my gratitude to the DESY directorate for partial support and for making DESY a challenging and sympathetic research environment.

## References

1. H. Abramowicz, *Int. J. Mod. Phys. A* **15S1**, 495 (2000), hep-ph/0001054.
2. F. Close, these proceedings, hep-ph/0110081.
3. A. Donnachie and P.V. Landshoff, *Nucl. Phys. B* **244**, 322 (1984).
4. J. Bartels and H. Kowalski, *Eur. Phys. J. C* **19**, 693 (2001), hep-ph/0010345.
5. D.E. Kharzeev *et al.*, *Nucl. Phys. A* **690**, 621 (2001), hep-ph/0007182.
6. E. Witten, *Adv. Theor. Math. Phys.* **2**, bf 505 (1998), hep-th/9803131.
7. ZEUS Collab., paper 954 submitted to EPS01, Budapest, Hungary, July 2001.
8. ZEUS Collab. J. Breitweg *et al.*, *Eur. Phys. J. C* **14**, 213 (2000), hep-ex/9910038.
9. ZEUS Collab., paper 548 submitted to EPS01, Budapest, Hungary, July 2001.
10. UA8 Collab., R. Bonino *et al.*, *Phys. Lett. B* **211**, 239 (1988).
11. G. Ingelman and P.E. Schlein, *Phys. Lett. B* **152**, 256 (1985).
12. M. Grazzini *et al.*, *Nucl. Phys. B* **519**, 394 (1998), hep-ph/9709452. J.C. Collins, *Phys. Rev. D* **57**, 3051 (1998), hep-ph/9709499.
13. L. Trentadue and G. Veneziano, *Phys. Lett. B* **323**, 201 (1994). A. Berera and D.E. Soper, *Phys. Rev. D* **50**, 4328 (1994), hep-ph/9403276. J. Blumlein and D. Robaschik, *Phys. Lett. B* **517**, 222 (2001), hep-ph/0106037.
14. J. Collins, hep-ph/0106126 and ref. therein.
15. ZEUS Collab, M. Derrick *et al.*, *Z. Phys. C* **73**, 253 (1997), hep-ex/9609003.
16. P. Van Esch *et al.*, *Nucl. Instrum. Meth. A* **386**, 310 (1997), hep-ex/0001046.
17. ZEUS Collab., M. Derrick *et al.*, *Phys. Lett. B* **315**, 481 (1993).
18. ZEUS Collab., J. Breitweg *et al.*, *Eur. Phys. J. C* **6**, 43 (1999), hep-ex/9807010.
19. H1 Collab., paper 808 submitted to EPS01, Budapest, Hungary, July 2001.
20. K. Golec-Biernat and M. Wüsthoff, *Phys. Rev. D* **60**, 114023 (1999), hep-ph/9903358.
21. K. Golec-Biernat and M. Wüsthoff, *Eur. Phys. J. C* **20**, 313 (2001), hep-ph/0102093.
22. W. Buchmüller *et al.*, *Nucl. Phys. B* **487**, 283 (1997), hep-ph/9607290.
23. ZEUS Collab., paper 566 submitted to EPS01, Budapest, Hungary, July 2001.
24. ZEUS Collab., J. Breitweg *et al.*, *Eur. Phys. J. C* **1**, 81 (1998), hep-ex/9709021.
25. H1 Collab., C. Adloff *et al.*, *Z. Phys. C* **76**, 613 (1997), hep-ex/9708016.
26. H1 Collab., C. Adloff *et al.*, *Eur. Phys. J. C* **20**, 29 (2001), hep-ex/0012051.
27. H. Jung, *Comp. Phys. Comm.* **86**, 147 (1995).
28. ZEUS Collab., S. Chekanov *et al.*, *Phys. Lett. B* **516**, 273 (2001), hep-ex/0107004.
29. H. Kowalski, DESY 99-141 (1999).
30. CDF Collab., T. Affolder *et al.*, *Phys. Rev. Lett.* **84**, 5043 (2000).
31. A.B. Kaidalov *et al.*, *Eur. Phys. J. C* **21**, 521 (2001), hep-ph/0105145, and ref. therein.
32. J.A. Crittenden, DESY-97-068, hep-ex/9704009.
33. L. Frankfurt *et al.*, *Phys. Rev. D* **54**,

- 3194 (1996), hep-ph/9509311.
34. M.G. Ryskin *et al.*, *Z. Phys. C* **76**, 231 (1997), hep-ph/9511228.
  35. A.D. Martin *et al.*, *Phys. Rev. D* **55**, 4329 (1997), hep-ph/9609448.
  36. H1 Collab., C. Adloff *et al.*, *Phys. Lett. B* **483**, 360 (2000), hep-ex/0005010.
  37. ZEUS Collab., presented by B. Mellado at EPS01, Budapest, Hungary, 2001.
  38. M. Diehl, SLAC-PUB-8670, hep-ph/0010200 and ref. therein.
  39. H1 Collab., C. Adloff *et al.*, *Phys. Lett. B* **517**, 47 (2001), hep-ex/0107005.
  40. ZEUS Collab., paper 564 submitted to EPS01, Budapest, Hungary, July 2001.
  41. Frankfurt *et al.*, *Phys. Rev. D* **58** 114001 (1998), hep-ph/9710356.
  42. A. Donnachie *et al.*, *Phys. Lett. B* **502**, 74 (2001), hep-ph/0010227.
  43. A. Hebecker and T. Teubner, *Phys. Lett. B* **498**, 16 (2001), hep-ph/0010273.
  44. L. Lukaszuk and B. Nicolescu, *Lett. Nuov. Cim.* **8**, 405 (1973).
  45. J. Bartels *et al.*, *Eur. Phys. J. C* **20**, 323 (2001), hep-ph/0102221.
  46. E.R. Berger *et al.*, *Eur. Phys. J. C* **14**, 673 (2000), hep-ph/0001270.
  47. H1 Collab., paper 795 submitted to EPS01, Budapest, Hungary, 2001.

## Discussion

B. Ward, MPI Munich and Univ. of Tennessee: You showed that the model of Golec-Biernat and Wüsthoff fits the data better without DGLAP evolution, but you did not say what conclusion you draw from this. What is your conclusion?

Answer: In the original version of the model, the dipole cross section, which contains the dynamics, was postulated without any assumption on the evolution, and the three free parameters of the model were determined by a fit to inclusive DIS data. Therefore, the agreement of the model with diffractive data, obtained using those parameters, can be regarded as a prediction. The fact that the model modified to include DGLAP evolu-

tion gives a worse description of the diffractive data if the same parameters are used, might indicate either that those parameters are no more adequate or that terms beyond the DGLAP equation are needed in the evolution.